Nanoscale

Accepted Manuscript

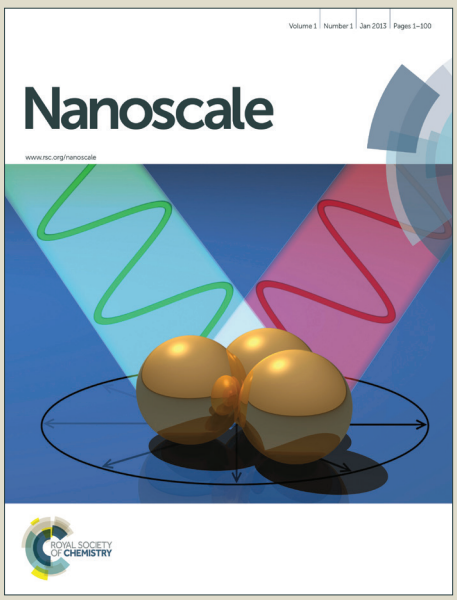

ROYAL SOCIETY OF CHEMISTRY

www.rsc.org/nanoscale

Graphic abstract

for

A general quantitative pH sensor developed with dicyandiamide *N*- doped high quantum yield graphene quantum dots †

Zhu Lian Wu[a], Ming Xuan Gao[a], Ting Ting Wang[b] , XiaoYan Wan[b], Lin Ling Zheng[a],

Cheng Zhi Huang*[a,b]

[a] *Education Ministry Key Laboratory on Luminescence and Real-Time Analysis, School of Chemistry and Chemical Engineering, Southwest University, Chongqing 400715, China. E-mail: chengzhi@swu.edu.cn, Tel: (+86) 23 68254659, Fax: (+86) 23 68367257.*

[b] *College of Pharmaceutical Science, Southwest University, Chongqing 400716, China*

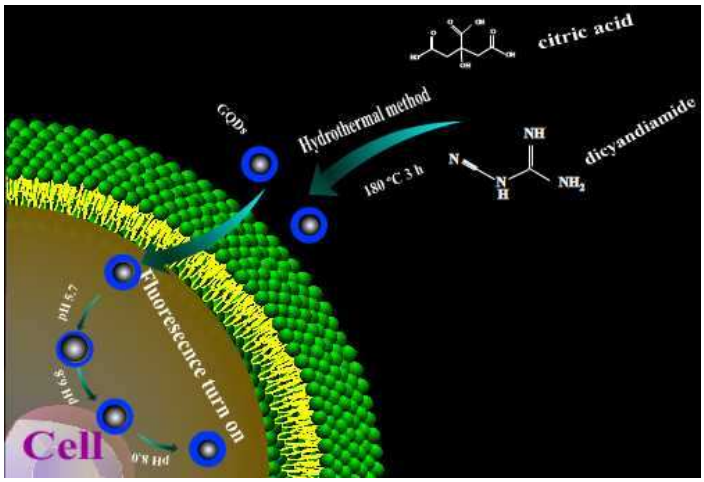

By taking citric acid as carbon source and dicyandiamide as N source through facial hydrothermal synthesis, we fabricated *N*-doped graphene quantum dots (GQDs), which possess excellent photolumincent properties with a high quantum yield of 36.5%, low toxic, photostable and pH- sensitive ranging from 1.81 to 8.96, and developed a pH sensor with wide range of applications across from real water to intracellular contents.

Cite this: DOI: 10.1039/c0xx00000x

www.rsc.org/xxxxxx

ARTICLE TYPE

A general quantitative pH sensor developed with dicyandiamide *N*- doped high quantum yield graphene quantum dots †

Zhu Lian Wu[a], Ming Xuan Gao[a],Ting Ting Wang[b], Xiao Yan Wan[b], Lin Ling Zheng[a], Cheng Zhi Huang*[ab]

Received (in XXX, XXX) Xth XXXXXXXXX 20XX, Accepted Xth XXXXXXXXX 20XX
DOI: 10.1039/b000000x

A general quantitative pH sensor across from environments to the life basic elements was developed by facial hydrothermal preparation of dicyandiamide (DCD) *N*-doped high quantum yield (QY) graphene quantum dots (GQDs) by taking citric acid (CA) as carbon source. The obtained *N*-doped GQDs have excellent photoluminesent (PL) properties with a relatively high QY of 36.5%, identifying *N*-doped chemistry could promote the QY of carbon nanomaterial. The possible mechanism for the formation of the GQDs is that the CA self-assembled into nanosheets structure through the intermolecular H-bonding at the initial stage of reaction and then, the pure graphene core with lots of function groups formed through the dehydration between carboxyl and hydroxyl of the intermolecules under hydrothermal condition. These *N*-doped GQDs are low toxic, photostable and pH- sensitive ranging from 1.81 to 8.96, giving a general pH sensor with wide range of applications across from real water to intracellular contents.

Introduction

pH is of great concern to all life forms. It has been well known that very small variations of pH will devastate lives of plants and animals. In our surroundings, acid rain, excessive human activities and untreated sewage will cause the environmental pH change and the acidification of soils, streams, lakes and seawater, which will further pollute our drinking water. Thus, monitoring the pH level of our environment is crucial.[1] In life science, on the other hand, intracellular pH is an essential parameter for cell, enzyme, and tissue activities, which plays a vital role in cell metabolism processes, such as the proliferation and apoptosis. [2] As abnormal intracellular pH values related to improper cell function and growth, may affect human physiology such as cancers and neurological disorders.[3] Therefore, the accurate estimation of pH values across from environments to the life basic elements is very important either in environmental, biomedical, or bioprocess applications.[4]

Among various developed techniques to measure pH, fluorescence-based ones have drawn much attention because they enjoy superb sensitivity, rapidity, and applicability to a wide variety of cells, etc.[5] Organic dyes,[1] functionalized boron nitride nanotubes, [6] quantum dots [3] and carbon dots, [7-9] have been successfully applied as the fluorescent pH sensors. They are very excellent for pH sensing, but some space there still should be promoted, such as range of response, linear relation for quantify, and avoiding complex modify process. The carbon dots, a superstar in carbon nanomaterial family, possess excellent optical properties such as stable photoluminescence, tunable luminescence emission, chemical inertness, favorable biocompatibility, which are advantages over heavy-metal-based quantum dots and the dye-based fluorescence probes used for imaging and sensing.[10] Graphene quantum dots (GQDs), as a recently developed kind of carbon dots, have much more special physical properties since they hold the structure of grapheme, and thus, they provide diverse promising applications in bioimaging, drug delivery, sensors, specially photocatalysis and optoelectronic devices.[11, 12]

Up to now, there are two main strategies for synthesizing variously sized GQDs, namely, top-down and bottom-up. The former strategy generally refers to the cutting of chunks of carbonaceous materials into GQDs by using physical or chemical methods, consisting of chemical ablation from graphene,[13] electrochemical synthesis,[14] and oxygen plasma treatment;[15] while the later one involves the synthesis of graphene moieties from molecular precursors. The approaches consist, for example, of the cage-opening of fullerene,[16] and solution chemistry methods.[17-19] Compared to top-down strategy, however, it's much easy for bottom-up strategy to control the size and shape of GQDs. So, the bottom up methods has been mostly adopted in the synthesis of GQDs. [11] Even though, the photoluminescence QY of the GQDs is quite low if no further passivation and/or doping made. Recently, there are some studies on preparation of *N*-doping GQDs-a relatively easy method for improving the QY, which have a comparatively high QY and excellent PL properties. [13,20, 21, 22] Consequently, *N*-doping is an effective method to synthesize GQDs with high QYs.

Herein, we reported a facile hydrothermal route to synthesize *N*-doped GQDs by using citric acid (CA) as carbon source and dicyandiamide (DCD) as N source, respectively. That further identify the *N*-doped chemistry might generate high photoluminescence QYs and introduce many functional groups. The process for the formation of the GQDs is showed in the scheme 1. The possible theory for the formation of the GQDs is that the CA self-assembled into nanosheets structure through the intermolecular H-bonding at the initial stage of reaction and then,

the pure graphene core with lots of function groups formed through the dehydration between carboxyl and hydroxyl of the intermolecules under hydrothermal condition. [23, 24] During, the -NH_2 group of dicyandiamide reacted with carboxyl or hydroxyl group of the graphene nanoparticles to form *N*-doped GQDs.[25]

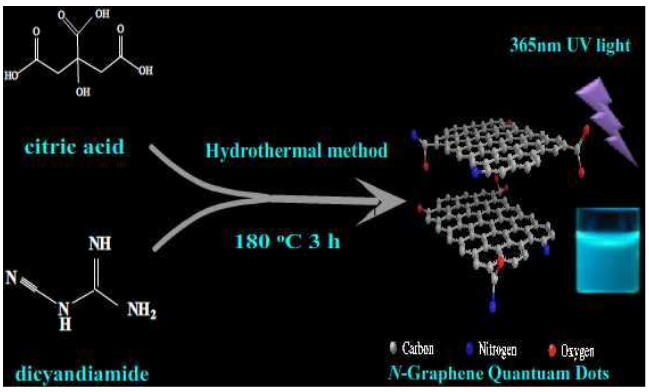

Scheme 1 Illustration of the formation process of GQDs from citric acid and dicyandiamide by hydrothermal treatment.

Experimental

Apparatus

The fluorescence and UV-vis absorption spectroscopy ware scanned with an F-2500 fluorescence spectrophotometer (Hitachi, Tokyo, Japan), and a UV-3600 spectrophotometer (Hitachi, Tokyo, Japan), respectively. High-resolution TEM (HRTEM) images and fast Fourier transform (FFT) spot diagram of GQDs were recorded with a high resolution transmission electron microscopy (Tecnai G2 F20 S-TWIN, FEI Company, USA), which was operated at an accelerating voltage of 200 kV. Elemental and functional groups analysis were made on ESCALAB 250 X-ray photoelectron spectrometer and FTIR-8400S Fourier transform infrared spectrometer (Tyoto, Japan) respectively. Zeta potential was measured by dynamic laser light scattering (ZEN3600, Malvern). The Raman spectrum of as-obtained sample on the Ag substrate was recorded on a LabRAM HR800 Laser confocal Raman spectrometer at ambient temperature (about 25°C). The fluorescence life time was measured with FL-TCSPC fluorescence spectrophotometer (Horiba Jobin Yvon Inc., France). Atomic force microscopy (AFM) images were captured on the Dimension Icon Scan Asyst atomic force microscope (Bruker Co.). X-ray diffraction (XRD) pattern was obtained by using an XRD-7000 with Cu Kα-radiation source. Fluorescence imaging was conducted on a DSU live-cell confocal microscope (Olympus, Japan) system with laser excitations of DAPI.

Synthesis of the fluorescent carbon dots

0.07g (0.33 mmol) citric acid and 0.25g (3 mmol) dicyandiamide were weighted and dissolved into 4.0 ml water, then the solution was transferred into a 25-mL Teflon-lined stainless-steel autoclave and heated at 180 ° C for 3 h. After the reaction completed, the autoclave was cooled down naturally. Next, the aqueous solution was centrifuged at 12000 rpm for 15 min to dislodge the non-fluorescent deposit and got the upper CDs aqueous solution for use. Through a dialysis membrane (1000 MWCO), residual citric acid, dicyandiamide and Fluorescent precursors will be detached for 48h. GQDs were then concentrated by freeze (-80 °C) and dried under vacuum.

Cytotoxicity investigation

The 2×10^6cells/mL Human epidermoid cancer cells (Hep-2) in Roswell Park Memorial Institute 1640 (RPMI 1640) supplemented with 10 % fetal bovine serum were added to each well of a 96-well plate (100 μL / well). The cells were cultured first for 24 h in an incubator (37°C, 5 % CO_2), and for another 24 h after the culture medium was replaced with 100 μL of RPMI 1640 containing 10 μL of the CDs at different doses(0, 0.2, 0.4, 0.6, 0.8, 1 mg·mL^{-1}). Then, followed by removing the culture medium, 10 μL of Cell Counting Kit-8 (CCK-8)solution was added to every cell well which was washed with PBS buffer twice and contained RPMI 1640 90 μL. The cells were further incubated for 1 h. The optical density (OD) of the mixture was measured at 450 nm with a Microplate Reader Model. The cell viability was estimated according to the following equation:

$$\text{Cell viability [\%]} = (\text{OD treated} / \text{OD control}) \times 100 \quad (1)$$

Wherein OD control was obtained in the absence of CDs, and OD treated obtained in the presence of CDs.

pH-dependent intracellular fluorescence imaging

The Hep-2 cells in Roswell Park Memorial Institute 1640 (RPMI 1640) supplemented with 10 % fetal bovine serum were added to each well of a 24-well plate (300 μL / well). The cells were cultured first for 24 h in an incubator (37 ˚C, 5 % CO2), and for another 24h after the culture medium was replaced with 270 μL of RPMI 1640 containing 30 μL CDs (at the concentration of 0.5 mg·mL^{-1}) . After that, the medium was removed and the cells were treated with nigericin (5 mg·mL^{-1}) in PBS (2 mL) for further 10 min. Before imaging, the GQDs loaded cells were rinsed three times and incubated with 1 mL PBS buffer (0.2 M) at various pH values (pH = 5.7, 6.8, 8.0) for 10 min, respectively. Cells were imaged with a DSU live-cell confocal microscope (Olympus, Japan) system with laser excitations of DAPI, and images were analyzed using Image-Pro Plus software.

Results and discussion

Characterizations of as-obtained GQDs

The morphology of the GQDs was characterized using transmission electron microscopy (TEM) and atomic force microscopy (AFM). Drops of a dilute aqueous solution of the GQDs were deposited on a carbon-coated copper grid for TEM and on mica substrates for AFM. The TEM image shows that GQDs are well dispersed (Fig. S1a, ESI†).The average size of the GQDs is about 2.3 nm with a relatively narrow size distribution between 1 and 4 nm (Fig.1a) and The high resolution TEM (HRTEM) image (Fig.1b)clearly shows the lattice spacing of 0.34 nm which is similar to (002) facet of graphitic carbon. The fast Fourier transform (FFT) spot diagram reveals the crystalline structure of GQDs. [26] AFM image (Fig.1c)shows that the height

of GQDs approximately is 0.4 - 0.7 nm about 1-2 graphene layers. Simultaneously, the three-dimension AFM image (Fig. S1b, ESI†) reveals that the GQDs have a uniform distribution in height.

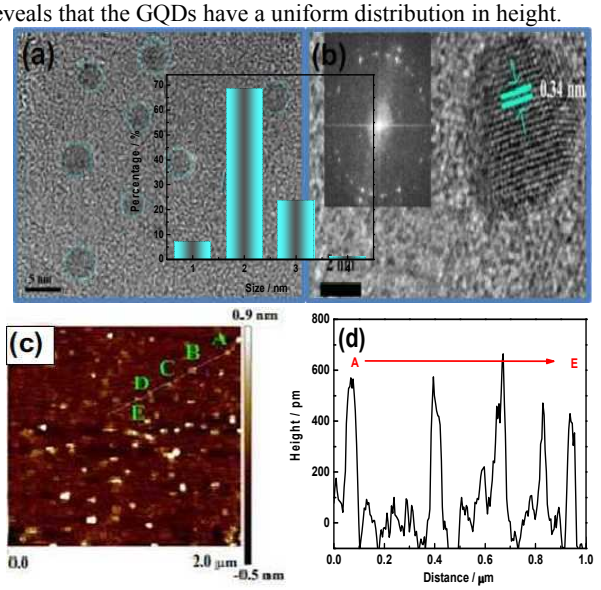

Fig.1 (a , b) HRTEM images of GQDs ,inset: size distribution and FFT image of the GQDs. (c) The AFM image and (d) the height distribution of GQDs

The XRD pattern of the GQDs (Fig.2a) displays a broad peak centered at 25°,similar to the graphite lattice spacing, which is attributed to highly disordered carbon atoms.[27] The Raman spectrum of the GQDs (Fig.2b) obtained under the Ag substrate (excited by 532 nm laser) displays two broad peaks at around 1360 cm^{-1} and 1604 cm^{-1}, which are attributed to the disordered D band and the crystalline G band. The relative intensity (I_D/I_G) of the characteristic bands for GQDs is around 0.86, thus indicating that they have a similar structure to graphite and are highly crystalline.[25]X-ray photoelectron spectroscopy (XPS) was performed to determine the composition of the GQDs. The full scan XPS spectrum of GQDs (Fig.2c) shows the existence of carbon (C 1s, 285 eV), nitrogen (N 1s, 400 eV) and oxygen (O 1s, 533 eV). There are four peaks in the high resolution scan of the C 1s region, indicating that carbon presents in four different chemical environments, corresponding to sp^2 C (C–C or C=C)in graphene at 284.8 eV, sp^3 C from C–N and C–O at 285.5 eV, C=N at 287.1 eV, and C=O at 288.7 eV.[28, 29] (Fig.S2a, ESI†) The O 1s spectrum of the GQDs presents two peaks, which are assigned to C=O at 531.6 eV and C–OH at 532.9 eV. (Fig.S2b, ESI†)As Fig.2d shows there are two peaks at 400.1 and 401.4 eV in the N 1s spectrum, which are attributed to the pyrrole-like N (C–N–C) and graphitic N or N–H bands, respectively.[30]

The surface functional groups of the GQDs are detected by Fourier transformed infrared (FTIR). The absorption band at 3441 cm^{-1} is assigned to O–H and N–H stretching vibrations of amine groups. The absorption band at 2900 cm^{-1} is attributed to C–H stretching vibrations, 2200-1900 cm^{-1} is assigned to C=N stretching vibration and 1600–1700 cm^{-1} is C=O stretching vibrations. Absorption band from1400 cm^{-1} is assigned to C–N stretching vibrations. The ν (C=O) and ν (C–N) peaks indicate the formation of amide bonds on the GQDs surface.[31] However,

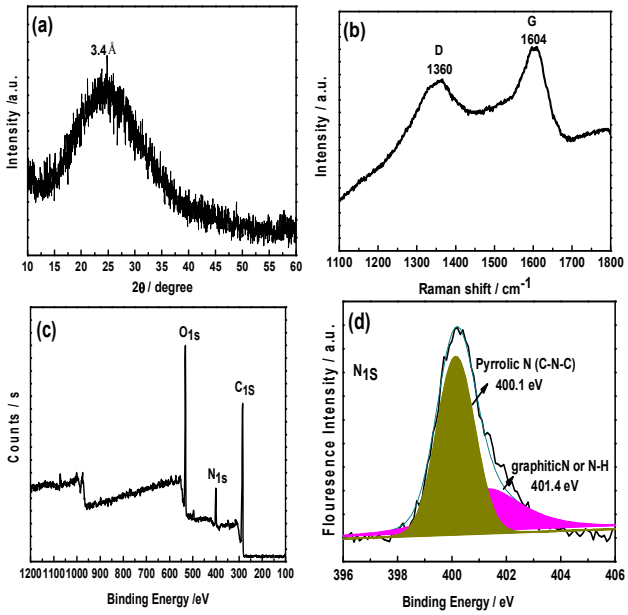

Fig.2 (a) XRD, (b) Raman, (c) XPS and (d) N 1s spectra of the products thus obtained.

some function groups from the raw materials have disappeared such as C≡N in DCD under the hydrothermal condition. (Fig.S3, ESI†) As shown from FTIR and XPS, the synthesized GQDs have various functional groups like –COOH, –OH and $–NH_2$, which improve the hydrophilicity and stability of the GQDs in aqueous system. Thus, the dicyandiamide plays three key roles in the hydrothermal process: as the precursor for *N*-doping, the passivation agent and providing a basic reaction environment with high pressure for dicyandiamide decomposing NH_3 at about 80 °C. All these greatly contribute to the formation and PL enhancement of GQDs.[32] The zeta potential of the GQDs in the aqueous solution is -12.7 mV, (Fig.S4, ESI†) owing to –COOH groups on the surface, indicating the GQDs are highly dispersed and stable in the aqueous system.[27]

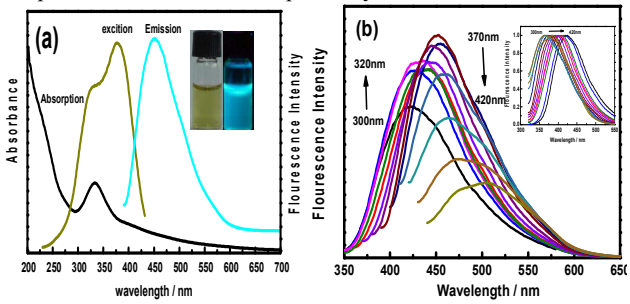

Fig.3 UV-vis absorption spectra and PL spectra of GQDs. (a) The emission spectrum was obtained under maximum excitation at 370 nm, and the excitation spectrum was obtained at the maximum emission wavelength of 452 nm. Inset: photographs taken under daylight (left) and 365 nm UV light (right). (b) Emission spectra of GQDs recorded for progressively longer excitation wavelength in 10 nm increment from 300 nm to 420 nm. Inset: the normalized PL emission spectra.

The absorption spectrum shows a clear absorption band at 333 nm with a little band at 234 nm. The peak at 234 nm, consistent with the π-> π* transition of C=C, results in nearly no observed PL emission. [33] The other centered at about 333 nm due to *n*->π* transition, namely, the trapping of excited-state energy by the surface states, leads to a strong emission.[34] The maximum

excitation wavelength is 370nm with a shoulder peak at about 320nm, which may be due to a transition from the σ and π orbital (HOMO) to the lowest unoccupied molecular orbital (LUMO),[35] and the maximum emission wavelength centered at 452nm. Very bright blue-green luminescence under the illumination of UV (365 nm) light, can be clearly seen in the inset of Figure 3a. The emission wavelengths of the GQDs depend on the excitation wavelengths. With increasing excitation wavelengths, the emission peaks shift to longer wavelengths and the intensity decreases, which is a common phenomenon observed in carbon-based fluorescent materials. There are two segments in the PL spectra with the maximum intensity at 320 and 370 nm, respectively, which is in accordance with the two peaks of excitation spectrum. (Fig.3b) Meanwhile, the GQDs have a good PL behavior with a high quantum yield of 36.5% against the reference of quinine sulfate. (Fig.S5, ESI†) In order to make clear the PL mechanism of the GQDs, different molar ratios of CA and DCD were used as materials to react through hydrothermal method at 180°C for 3h. As the molar of DCD is more than that of CA, the products from them show stronger PL intensity, but only CA, DCD or the molar of CA is more than that of DCD, the products almost show no PL emission. (Fig.S6, ESI†)As our described experimental results above, we argue that the strong PL emission of the GQDs mainly result from the surface-doped nitrogen atom, in other words, the PL emission from the function groups on the GQDs surface, assembling the PL mechanism of organic dyes.[27] Additionally, the average fluorescence lifetime of GQDs was calculated as 4.78 ns, (Fig.S7, ESI†) such a short lifetime also indicates that the possible luminescent mechanism is the radioactive recombination nature of excitations.[36]

As scheme 2 illustrates the possible mechanism of luminescence is that the electrons in GQDs excited by illuminant in the external environment, jump from a fundamental electronic state S_0 to the various vibrational energy level of the first excited singlet state S_1 (marked as V_1, V_2 and V_3…), then through internal conversion, the electrons come back to S_1. After that, some energy is absorbed by the energy trap and some is emitted in the form of photons, meanwhile, the protons return S_0.

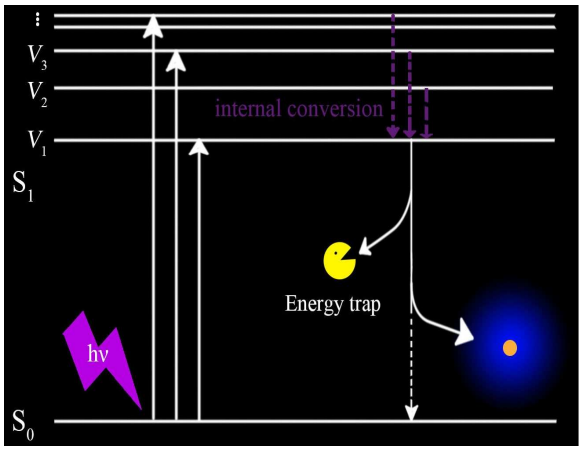

Scheme 2 The possible luminescent mechanism of the as-obtained GQDs.

Stability of the as-prepared GQDs

The obtained GQDs show excellent photostability, and the PL intensity keeps invariant, under continuous excitation (370 nm) with a Xe lamp for 30 min. (Fig.S8, ESI†) Meanwhile, the as-prepared GQDs are very stable, and the PL intensity scarcely shows any change even though they were dispersed in an aqueous solution with the ionic strength of 3.0 mol·L^{-1} NaCl, (Fig.S9, ESI†) indicating that GQDs could resist comparatively high ionic strength and not be to aggregate in thus medium. Interestingly, the GQDs possess the property of pH sensitive, and the PL intensity gets increase in the pH ranging from 1.89 to 11.98. (Fig.S10, ESI†) We also investigated their stability in complex systems such as serum, the fluorescence intensity of as-prepared GQDs increase a little in serum for slightly alkaline medium, which could be testified with three parallel blood samples. (Fig.S11, ESI†)

pH dependent optical properties of the GQDs

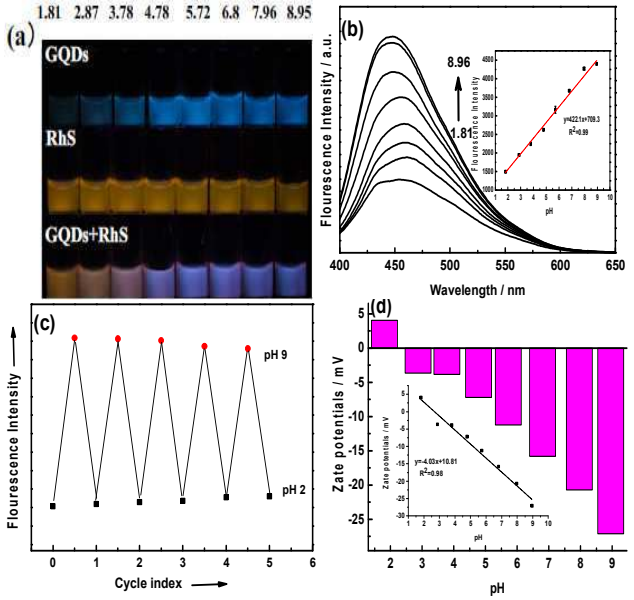

Fig.4 (a) The photograph of the GQDs, RhS (6 mg.mL^{-1}) and the mixed aqueous in different pH buffer from 1.81 to 8.95 under 365nm UV light. (b) The fluorescence intensity varied with different pH (1.81, 2.87, 3.78, 4.78, 5.72, 6.8, 7.96, and 8.95) BR buffer, c_{GQDs} = 62.7 μg.mL^{-1}. Inset: the linear relationship between fluorescence intensity and pH. (c) The pH reversibility study of GQDs between pH 2 and 9. (d) The Zeta potentials of GQDs in different pH buffer. Inset: the linear relationship between them.

The GQDs are pH-sensitive with a broad response region and the PL emission is switched off and on in the low and high pH regions. From the picture of Fig.4a, the clear increase of the PL intensity will be observed under 365 nm UV light with the pH from 1.81 to 8.95. To increase the color contrast, the pH-insensitive Rhodamine S (RhS) which presents yellow color under 365 nm UV light was mixed with the GQDs. The mixed aqueous shows different colors from yellow, pink to purple in different pH, which could give an amiable color signal to estimate pH. What's more, the fluorescence intensity of the GQDs has an excellent linear relationship with pH in this region, illustrating that the pH sensor could be used for quantitative measurement. (Fig.4b) Especially, the pH-response of the PL behavior of the GQDs displays a brilliant reversibility. As illustrated in Fig.4c that the PL intensity significantly enhances with the increase of

pH from 2 to 9. Afterwards, when changing back the pH from 9 to 2, the PL restores nearly as before. And even after 5 cycles of changing pH from 2 to 9 and then from 9 to 2 in the same solution by the concentrated NaOH and HCl, the PL intensity remains virtually unchanged. This observation indicates that PL species in the GQDs should have basic and acidic sites relevant to the photoluminescence emission. [37] To make clear the reason for this pH dependent PL emission, we investigate the relationship between the zeta potential and pH. As Fig.4d shows the zeta potential and the pH can be expressed as a simple linear equation y=-4.086pH+10.81 (y stands for the zeta potentials of GQDs in different pH buffers), which indicates that the reversible protonation and deprotonation of the function groups such as amide and carboxylic groups on the GQDs surface should be responsible for the variation of the PL feature. In the meantime, the linear equation gives an isoelectric point of the GQDs around 2.65. The as-prepared GQDs are positively charged when the pH is low 2.65, otherwise, negatively charged, which analogous to the property of amino acid.[38]

pH detection for environmental real water samples

The pH sensitive property for the PL emission of the GQDs could be applied in the pH detection of water body to make sure if the water is polluted or if it is safe to drink. Comparing the results from our method and 510 pH meter as table 1 shows, we realize the result is reliable and satisfied and the GQDs could be utilized as an excellent fluorescent pH indicator for real water samples. The pH sensitive behavior of the GQDs also exists in phosphate (PBS) buffer-a common buffer for cell culture, (Fig.S12, ESI†) which means that the GQDs will response for the intracellular pH change.

Table 1 Measurement of pH in real water samples.

Sample	pH_1	pH_2	R.S.D. (%, n=3)
River water	7.79	7.91	1.71
Rain water	6.63	6.55	1.28
Tap water	7.11	7.04	1.69

pH_1 measured by a EUTECH LNSTRUMENTS 510 pH meter; pH_2 obtained from the stander calibration curve of PL intensity and pH under the same condition of the fluorescence spectrophotometer.

Intracellular pH sensing by confocal microscopy

To further demonstrate the application of the probe in live cells, the inherent cytotoxicity of GQDs was evaluated using Human epidermoid cancer cells (Hep-2) lines through Cell Counting Kit-8 (CCK-8) assay. The cell viability does not significantly change upon treatment with GQDs with high dose of 1 mg·mL^{-1} for 24 h, (Fig.S13, ESI†) indicating that the obtained GQDs scarcely impose toxicity to the cells. Hence they are suitable for *in vivo* applications. The intracellular calibration experiment was made in GQDs-loaded Hep-2 cells with nigericin, which is a standard approach for homogenizing the pH of cells and culture medium.[9, 39] In the process of intracellular pH sensing, GQDs act two parts: the signal molecule for pH sensing and the carrier for carrying itself as a sigle molecule to enter the cells. This could refrain from fussy modification process. As the confocal images in Fig.5 (a-c) of Hep-2 cells treated with PBS buffer show the GQDs are well-distributed in live cells, indicating the excellent membrane permeability for their small size. The GQDs-loaded cells exhibit weak fluorescence in pH 5.7 PBS buffer for DAPI channel, nevertheless, the Hep-2 cells become brighter as the pH increases. The overlay images of confocal fluorescence microphotographs and bright ones in Fig.5 (d-f) also illustrate the GQDs could readily reveal the pH variations in Hep-2 cells by a fluorescence brightness response. We also chose four cells to observe their fluorescence intensity change with pH. As Fig.5g states that the fluorescence intensity of the four cells has the same change trend, that is, the fluorescence intensity increase with pH from 5.7,6.8 to 8.0. All these results establish that the obtained GQDs are desirable pH probe for monitoring the pH changes in live cells.

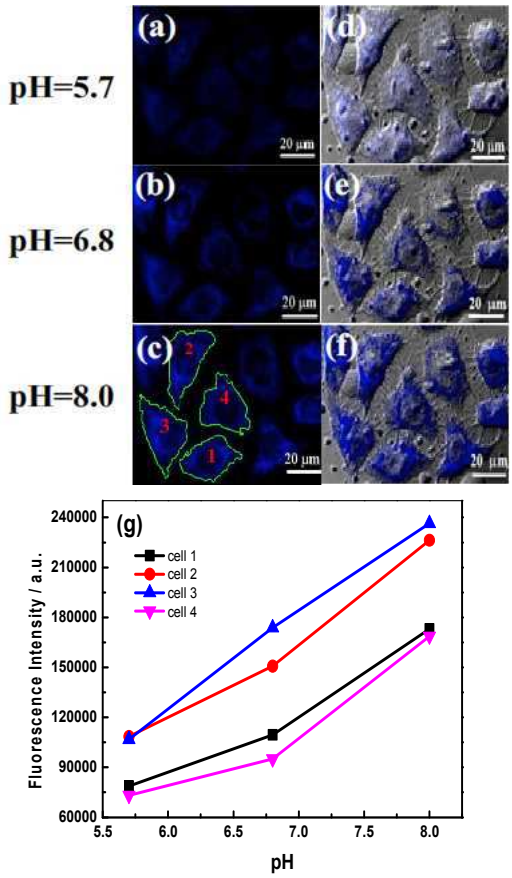

Fig.5 Confocal fluorescence images of Hep-2 cells after incubation with GQDs (0.5 mg.mL^{-1}) and nigericin and clamped in pH (a) 5.7, (b) 6.8, and (c) 8.0 PBS buffer, respectively. The overlay merges of a confocal fluorescence microphotograph and a bright microphotograph at pH (d) 5.7, (e) 6.8, and (f) 8.0, respectively. (g) The fluorescence intensity of the four cells (marked in the Fig 5c) change with different pH.

Conclusions

In summary, a facial hydrothermal method has been established to fabricate *N*-doped GQDs from CA and DCD. The as-prepared GQDs with high QY and attractive PL properties are able to resist acids, bases and higher ionic strength, even maintain

photostability in complex system such as serum. More interesting, the GQDs display pH-sensitive behavior and the fluorescence intensity has a nice linear relationship with the pH in a wide range from 2 to 9. In addition, the result of the cell toxicity experiment declares that they have good biocompatibility. So the GQDs could be used as a fluorescent pH indicator to monitor pH fluctuations both in aqueous solution and live cells, especially, the quantificational detection of the pH. Application of the GQDs for pH imaging in live Hep-2 cells was successfully achieved, proving that they can reveal intracellular pH fluctuations via a change of PL intensity response. We expect the GQDs could be unitized to quantify the intracellular pH in the future.

Acknowledgements

This work was financially supported by the National Natural Science Foundation of China (No. 21035005) and the Ministry of Science and Technology of the People's Republic of China (2011CB933600).

Notes and references

Education Ministry Key Laboratory on Luminescence and Real-Time Analysis, College of Chemistry and Chemical Engineering, Southwest University, Chongqing 400715, China. E-mail: chengzhi@swu.edu.cn, Tel: (+86) 23 68254659, Fax: (+86) 23 68367257.

[b] College of Pharmaceutical Science, Southwest University, Chongqing 400716, China

† Electronic Supplementary Information (ESI) available: Experimental section and additional figures (Fig.S1-S13). See DOI: 10.1039/b000000x/

1. Z. Y. Yang, W. Qin, J. W. Y. Lam, S. Chen, H. H. Y. Sung, I. D. Williams and B. Z. Tang, *Chem. Sci.*, 2013, **4**, 3725.
2. W. M, H. U, M. F and S. M., *Res. Exp.Med.*, 1998, **198**, 73.
3. A. M. Dennis, W. J. Rhee, D. Sotto, S. N. Dublin and G. Bao, *ACS Nano*, 2012, **6**, 2917.
4. H. R. Kermis, Y. Kostov, P. Harms and G. Rao, *Biotechnol. Prog.*, 2002, **18**, 1047.
5. Z. Bai, R. Chen, P. Si, Y. Huang, H. Sun and D.-H. Kim, *Appl. Mater. Interfaces*, 2013, **5**, 5856.
6. Q. Huang, Y. Bando, L. Zhao, C. Y. Zhi and D. Golberg, *Nanotechnology*, 2009, **20**, 415501.
7. L. M. Shen, L. P. Zhang, M. L. Chen, X. W. Chen and J. H. Wang, *Carbon*, 2013, **55**, 343.
8. X. F. Jia, J. Li and E. Wang, *Nanoscale*, 2012, **4**, 5572.
9. W. Shi, X. H. Li and H. M. Ma, *Angew. Chem. Int. Ed.*, 2012, **51**, 1.
10. S. N. Baker and G. A. Baker, *Angew. Chem. Int. Ed.*, 2010, **49**, 6726.
11. J. H. Shen, Y. H. Zhu, X. L. Yang and C. Z. Li, *Chem. Commun.*, 2012, **48**, 3686.
12. L. Li, G. Wu, G. Yang, J. Peng, J. Zhao and J.-J. Zhu, *Nanoscale*, 2013, **5**, 4015.
13. J. H. Shen, Y. H. Zhu, C. Chen, X. L. Yang and C. Z. Li, *Chem. Commun.*, 2011, **47**, 2580.
14. Q.-L. Zhao, Z.-L. Zhang, B.-H. Huang, J. Peng, M. Zhang and D.-W. Pang, *Chem. Commun.*, 2008, 5116.
15. T. Gokus, R. R. Nair, A. Bonetti, M. B. hmler, A. Lombardo, K. S. Novoselov, A. K. Geim, A. C. Ferrari and A. Hartschuh, *ACS Nano*, 2009, **3**, 3963.
16. D. V. Kosynkin, A. L. Higginbotham, A. Sinitskii, J. R. Lomeda, A. Dimiev, B. K. Price and J. M. Tour, *Nature*, 2009, **458**, 872.
17. I. P. Hamilton, B. Li, X. Yan and L.-s. Li, *Nano Lett.*, 2011, **11**, 524.
18. R. L. Liu, D. Q. Wu, X. L. Feng and K. Müllen, *J. Am. Chem. Soc.*, 2011, **133**, 15221.
19. Q. Q. Li, S. Zhang, L. M. Dai and L.- S. Li, *J. Am. Chem. Soc.*, 2012, **134**, 18932.
20. Y.-P. Sun, B. Zhou, Y. Lin, W. Wang, K. A. S. Fernando, P. Pathak, M. J. Meziani, B. A. Harruff, X. Wang, H. F. Wang, P. G. Luo, H. Yang, M. E. Kose, B. L. Chen, L. M. Veca and S.-Y. Xie, *J. Am. Chem. Soc.*, 2006, **128**, 7756.
21. S. Liu, J. Q. Tian, L. Wang, Y. W. Zhang, X. Y. Qin, Y. L. Luo, A. M. Asiri, A. O. Al-Youbi and X. P.Sun, *Adv. Mater.*, 2012, **24**, 2037.
22. J. Zhou, Y. Yang and C.-y. Zhang, *chem.Comm.,* 2013, **49**, 8605.
23. Y. Li, Y. Zhao, H. H. Cheng, Y. Hu, G. Q. Shi, L. M. Dai and L. T. Qu, *J. Am. Chem.Soc.*, 2012, **134**, 15.
24. Y. Q. Dong, J. W. Shao, C. Q. Chen, H. Li, R. X. Wang, Y. W. Chi, X. M. Lin and G. N. Chen, *Carbon*, 2012, **50**, 4738.
25. D. Qu, M. Zheng, P. Du, Y. Zhou, L. G. Zhang, D. Li, H. Q. Tan, Z. Zhao, Z. G. Xie and Z. C. Sun, *Nanoscale*, 2013.**DOI**: 10.1039/C3NR04402E
26. D. Qu, M. Zheng, P. Du, Y. Zhou, L. G. Zhang, D. Li, H. Q. Tan, Z. Zhao, Z. G. Xie and Z. C. Sun, *Nanoscale*, 2013.**DOI**: 10.1039/C3NR04402E
27. S. G. Qu, X. Y. Wang, Q. P. Lu, X. Y. Liu and L. J. Wang, *Angew. Chem. Int. Ed.*, 2012, **124**, 12381.
28. Y. Q. Dong, H. C. Pang, H. B. Yang, C. X. Guo, J. W. Shao, Y. W. Chi, C. M. Li and T. Yu, *Angew. Chem. Int. Ed* 2013, **52**, 1.
29. C. F. Wang, X. Wu, X. P. Li, W. T. Wang, L. Z. Wang, M. Gu and Q. Li, *J. Mater. Chem.*, 2012, **22**, 15522.
30. Z.-H. Sheng, L. Shao, J.-J. Chen, W.-J. Bao, F.-B. Wang and X.-H. Xia, *ACS Nano*, 2011, **5**, 4350.
31. X. Y. Zhai, P. Zhang, C. J. Liu, T. Bai, W. C. Li, L. M. Dai and W. G. Liu, *Chem. Commun.*, 2012, **48**, 7955.
32. Y. M. Guo, Z. Wang, H. W. Shao and X. Y. Jiang, *Carbon*, 2 0 1 3 **52**, 583.
33. B. G. Eda, Y.-Y. Lin, C. Mattevi, H. Yamaguchi, H.-A. Chen, I.-S. Chen, C.-W. Chen and M. Chhowalla, *Adv. Mater.* , 2010, **22**, 505.
34. X. Wang, L. Cao, S.-T. Yang, F. Lu, M. J. Meziani, L. L. Tian, K. W. Sun, M. A. Bloodgood and Y.-P. Sun, *Angew. Chem. Int. Ed.* , 2010, **49**, 5310 .
35. J. Peng, W. Gao, B. K. Gupta, Z. Liu, R. Romero-Aburto, L. H. Ge, Li Song, L. B. Alemany, X. B. Zhan, G. H. Gao, S. A. Vithayathil, B. A. Kaipparettu, A. A. Marti, T. Hayashi, J.-J. Zhu and P. M. Ajayan, *Nano Lett.*, 2012, **12**, 844.
36. P. Anilkumar, X. Wang, L. Cao, S. Sahu, J.-H. Liu, P. Wang, K. Korch, K. N. T. II, A. Parenzan and Y.-P. Sun, *Nanoscale*, 2011, **3**, 2023.
37. D. Y. Pan, J. C. Zhang, Z. Li, C. Wu, X. M. Yan and M. H. Wu, *Chem. Commun.*, 2010, **46**, 3681.
38. Z. L. Wu, P. Zhang, M. X. Gao, C. F. Liu, W. Wang, F. Leng and C. Z. Huang, *J. Mater. Chem. B*, 2013, **1**, 2868.
39. P. S. Song, X. T. Chen, Y. Xiang, L. Huang, Z. J. Zhou, R. R. Wei and A. J. Tong, *J. Mater. Chem.*, 2011, **21**, 13470.